Spin Coupling in Engineered Atomic Structures

Cyrus F. Hirjibehedin,* Christopher P. Lutz, Andreas J. Heinrich

We used a scanning tunneling microscope to probe the interactions between spins in individual atomic-scale magnetic structures. Linear chains of 1 to 10 manganese atoms were assembled one atom at a time on a thin insulating layer, and the spin excitation spectra of these structures were measured with inelastic electron tunneling spectroscopy. We observed excitations of the coupled atomic spins that can change both the total spin and its orientation. Comparison with a model spin-interaction Hamiltonian yielded the collective spin configuration and the strength of the coupling between the atomic spins.

Meticulous control of the coupling between spins is central to the use of magnetic nanostructures in future spintronics (*1*) and quantum information devices (*2*). Such spin coupling has been studied recently in pairs of lithographically fabricated quantum dots (*3*, *4*). At the atomic length scale, a small number of spins can be coupled directly in metal-atom clusters (*5*) or chains (*6*) and through linker groups in molecular magnetic structures (*7*). Spin interactions in these systems typically have been probed using ensemble-averaging techniques, such as susceptibility measurements (*8*, *9*), electron paramagnetic resonance (*10*, *11*), and inelastic neutron scattering (*12*).

Individual atomic-scale magnetic structures can be studied with scanning probe techniques (*13*, *14*). The scanning tunneling microscope (STM) has been used to detect the Kondo interactions between conduction electrons and single atomic spins (*15*, *16*) and to study the properties of individual magnetic islands (*17*, *18*). Recently, inelastic electron tunneling spectroscopy (IETS) with an STM was used to measure the spin excitation spectra of individual magnetic atoms (*19*). Additionally, the STM can be used to manipulate and assemble individual nanostructures (*20*). Such atomic manipulation in situ was used to construct magnetic dimers and trimers, which displayed evidence of coupled-spin behavior (*21*, *22*).

We have combined the imaging and manipulation capabilities of the STM with its ability to measure spin excitation spectra at the atomic scale. We used an STM to build magnetic chains as long as 10 Mn atoms on a thin insulating layer and probed their collective spin excitations with IETS. The spectra depended strongly on both the parity and length of the chains, as well as the binding sites upon which the chains were built. We observed excitations that can change both the collective spin of the coupled system and the orientation of the spin with respect to a magnetic field. A quantitative comparison with the Heisenberg open chain model allowed us to determine the antiferromagnetic (AF) coupling strength, which could be set at either 3 or 6 meV by selecting the precise atomic configuration. In addition, the spin of the Mn atoms in the chains was found to be ½.

Experiments were conducted with ultrahigh-vacuum, low-temperature STMs reaching base temperatures of 5.5 and 0.6 K. In the latter STM, we applied magnetic fields up to $B = 7$ T in the plane of the sample, oriented ~55° from the chains. We measured differential conductances dI/dV using lock-in detection of the tunnel current I by adding a 20 to 50 μV_{rms} modulation at 732 Hz to the sample bias voltage V.

To date, spin excitations have been observed with IETS only when the atomic spins were separated from the metal surface by a thin insulating layer (*19*). Here we used the insulating properties of a single atomic layer of copper nitride (*23*, *24*), which we denote as CuN. A small island of CuN surrounded by bare Cu(100) is shown in Fig. 1A, along with the assigned positions of the surface atoms. The relatively simple structure of these islands offers a well-characterized environment in which to assemble nanostructures.

Prior STM studies using thin insulating layers (*19*, *25*–*27*) did not report the ability to precisely position atoms or molecules. We have developed a vertical transfer technique (*28*, *29*) to manipulate Mn atoms on the CuN surface with atomic precision (*30*). In the atom-by-atom construction of a chain of 10 Mn atoms on a

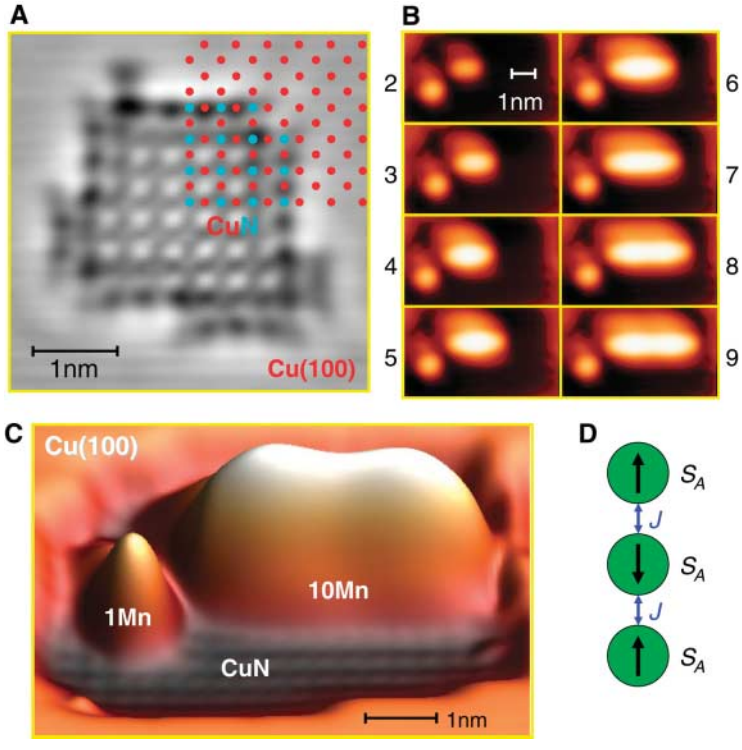

Fig. 1. Mn chains on CuN. (**A**) STM constant-current topograph (10 mV, 1 nA) of a CuN island on Cu(100). Topograph is high-pass (curvature) filtered to enhance contrast, with lattice positions of Cu (red dots) and N (blue dots) atoms overlaid. CuN islands appear as 0.14-nm depressions for $|V| < 0.1$ V. (**B**) STM images of the building of a chain of Mn atoms, lengths 2 to 9, on CuN (10 mV, 0.1 nA). The Mn atom in the lower left of each image appears as a bump 0.34 nm high. The dimer has a smaller peak height of 0.30 nm. Chains of four or more atoms have peak heights of ~0.45 nm. Individual atoms in the chain cannot be resolved. Artifacts seen to the upper left of all structures are characteristic of the atomic arrangement of the tip used for manipulation. (**C**) Perspective rendering of a chain of 10 Mn atoms. The observed double-peak structure suggests the existence of one-dimensional delocalized electronic states as seen in metallic chains constructed on metal surfaces (*38*). (**D**) Schematic of the AF coupling of three atomic spins described by the Heisenberg model in Eq. 1.

IBM Research Division, Almaden Research Center, 650 Harry Road, San Jose, CA 95120, USA.

*To whom correspondence should be addressed. E-mail: hirjibe@us.ibm.com

CuN island (Fig. 1, B and C), the Mn atoms were positioned atop Cu atoms in the CuN so that one N atom lay between each pair of Mn binding sites. As a result, the Mn atoms were spaced 0.36 nm apart.

The *dI*/*dV* spectra of Mn chains of 1 to 10 atoms at $B = 0$ (Fig. 2) displayed a striking dependence on the parity of the chain. At voltages below 1 mV, the spectra of odd-length chains, including the single Mn atom, exhibited a narrow dip in conductance that was centered at 0 V. This feature was absent in all even-length chains. At larger energies, both odd and even chains, with the exception of single Mn atoms, showed large steps in conductance at voltages that were symmetric with respect to zero. These steps were more pronounced in the long even-length chains: The change in conductance across these steps was almost a full order of magnitude. The energies of these steps were largest for the dimer and trimer, and they decreased with chain length for chains of the same parity. The conductance steps occurred at the same energy when the spectra were measured at different locations along the length of the chains, which suggests that these steps are properties of the entire chain rather than of any one atom or part of the chain.

We used IETS (*31*, *32*) to interpret the steps in the *dI*/*dV* spectra of the chains. When a system with a mode at energy E is placed within a tunnel junction, electrons can excite this mode during the tunneling process only if the magnitude of the bias voltage V exceeds E/e (where $-e$ is the charge on the electron). This additional tunneling channel generally results in steps in conductance at $V = \pm E/e$.

To understand the IETS steps in Fig. 2, we focus first on the case of a single Mn atom. The *dI*/*dV* spectra on a single Mn atom on CuN as a function of magnetic field (Fig. 3) all exhibit a dip centered at $V = 0$ that we interpret as symmetric IETS steps in conductance, similar to the spin-flip excitations observed for Mn on aluminum oxide (*19*). A spin-flip excitation changes the magnetic quantum number m but leaves the total spin S unchanged. The steps in conductance shift to higher voltage with increasing magnetic field as described by $eV = \pm g\mu_B B$ with $g \sim 2$, where g is the Landé g value and μ_B is the Bohr magneton. The odd-length chains all show similar behavior around $V = 0$, as illustrated for the trimer in Fig. 3B. The existence of spin-flip excitations requires $S > 0$ for the ground state of these chains. In contrast to previous work (*19*), the spin-flip excitations seen in Fig. 3A deviate at low magnetic fields from the expected energy of $g\mu_B B$: As seen in Fig. 2, a spin-flip excitation is present even at $B = 0$ in the odd-length chains. This zero-field splitting grows in energy with increasing chain length and is likely caused by magnetocrystalline anisotropy arising from the loss of rotational symmetry at the surface (*33*, *34*).

None of the even-length chains exhibited a spin-flip excitation: the spectra are flat near $V = 0$, both at $B = 0$ and at fields up to $B = 7$ T (Fig. 4A). The absence of the spin-flip excitation on the even-length chains is consistent with a ground-state spin $S = 0$. The alternation of the ground-state spin between zero for even-length chains and nonzero values for odd-length chains indicates AF coupling between the atomic spins.

For the even-length chains in Fig. 2, we interpret the lowest energy conductance steps as excitations that change the total spin of the chain. The dimer's conductance spectra between 4 and 8 mV are shown as a function of magnetic field in Fig. 4A. The single step at 6 mV at zero field is split into three distinct steps at $B = 7$ T; we interpret these steps as three IETS excitations. The step energies, as determined by IETS fitting, are shown in Fig. 4B. The three excitations shift as $\Delta m g\mu_B B$ for $\Delta m = -1, 0, 1$ and $g = 2.1 \pm 0.1$. The emergence of three distinct excitations at large B that are essentially degenerate at $B = 0$ suggests that the first excited state for the even-length chains is a triplet state ($S = 1$). The IETS steps thus correspond to spin-changing transitions from the ground state (with $S = 0$ and $m = 0$) to an excited state (with $S = 1$ and $m = -1, 0, 1$) (Fig. 4C). We interpret the different zero-field energy of the $m = \pm 1$ and $m = 0$ excited states as another manifestation of magnetocrystalline anisotropy. A similar singlet-triplet excitation

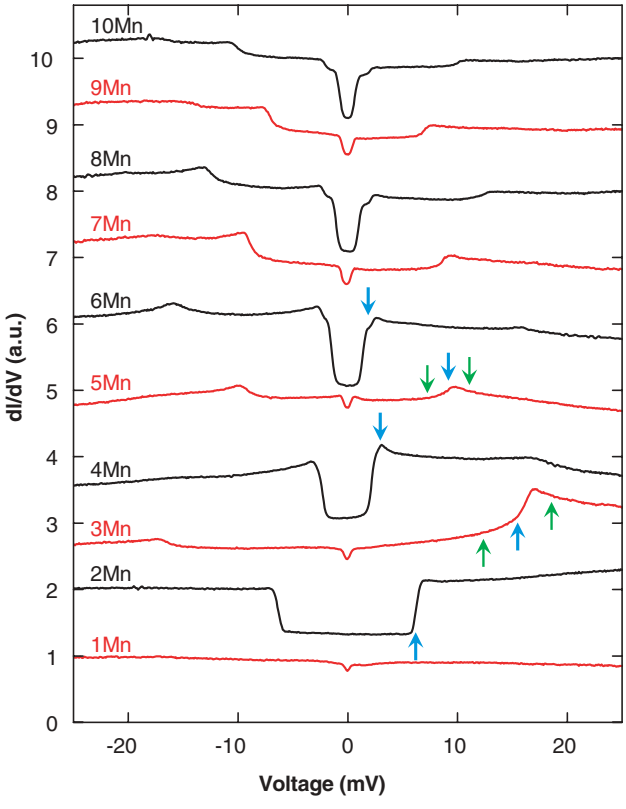

Fig. 2. Conductance spectra of Mn chains on CuN. Spectra were taken with the tip positioned above the center of chains of Mn atoms of lengths 1 to 10 at $T = 0.6$ K and $B = 0$ T. Spectra were acquired at a nominal junction impedance of 20 megohms (20 mV, 1 nA) and were not sensitive to junction impedance. Successive spectra are vertically offset by one unit for clarity. Odd spectra are in red and even spectra are in black to emphasize the parity dependence. Blue arrows indicate the lowest energy spin-changing excitation obtained from the Heisenberg model described in Eq. 1 with $J = 6.2$ meV and $S_A = ½$. For comparison, green arrows indicate the same excitation with $S_A = 2$ (lower voltage) and $S_A = 3$ (higher voltage) on the trimer and pentamer; the same excitation with $S_A = 2$ and $S_A = 3$ is not distinguishable from $S_A = ½$ on the dimer, tetramer, and hexamer chains.

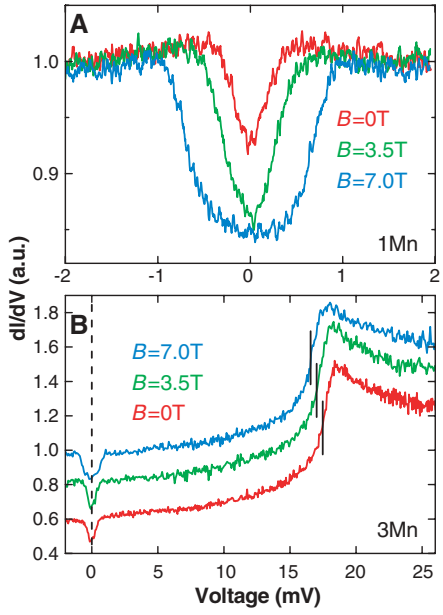

Fig. 3. Conductance spectra of Mn atom and trimer on CuN. (**A**) Spectra taken on a single Mn atom on CuN at $T = 0.6$ K at $B = 0$, 3.5, and 7.0 T. All spectra were acquired at a nominal junction impedance of 20 megohms (8 mV, 0.4 nA). (**B**) Spectra taken on a Mn trimer on CuN at $T = 0.6$ K at $B = 0$, 3.5, and 7.0 T. All spectra were acquired at a nominal junction impedance of 20 megohms (20 mV, 1 nA), and successive spectra are vertically offset by 0.2 units for clarity. Vertical lines highlight the shift of the high-energy step to lower energy with increasing magnetic field.

also occurs for the other even-length chains. As seen in Fig. 2, the zero-field splitting becomes more pronounced in the longer even-length chains, where two distinct steps are well resolved even at $B = 0$.

We analyze our spectroscopic results by using the Heisenberg model for an open chain of N coupled spins. In its simplest form, this model neglects any zero-field splitting and includes only identical nearest neighbor exchange interactions (coupling strength J) between the spins (Fig. 1D). We assume that all sites have the same spin S_A. The Hamiltonian is

$$H_N = J\sum_{i=1}^{N-1} \mathbf{S}_i \cdot \mathbf{S}_i + 1 \qquad (1)$$

where $\mathbf{S}_i$ is the spin operator for the ith site along the chain. The eigenvalue of $\mathbf{S}_i^2$ is thus $S_A(S_A + 1)$ for every i.

For a dimer, the ground state of the AF ($J > 0$) Heisenberg chain is a singlet ($S = 0$) and the first excited state is a triplet ($S = 1$) with energy separation J. This result is independent of the spin S_A of the constituent atoms. The energy spacing between the ground state and the first excited state provides a direct measure of the coupling strength J. For the dimer shown in Fig. 2, we determine $J = 6.2$ meV. We find that the value of J varies by ±5% for dimers in different locations on several CuN islands, as can be seen for the dimer in Fig. 4, which has $J = 5.9$ meV, and in fig. S1A, which has $J = 6.4$ meV.

In contrast to the dimer, the ground state of the Heisenberg AF trimer has total spin $S = S_A$. Generally, the first excited state has total spin $S_A - 1$ and is higher in energy by $S_A J$; the exception is the case of $S = ½$, where both the ground and first excited states have total spin ½. Figure 2 shows the energy of the first excited state for the trimer for a few possible values of S_A, where the value of J used was that determined from the dimer. The conductance step at ~16 mV, which we now assign to the lowest spin-changing transition, is best matched with the result for $S_A = ½$. The presence of a broad peak in the trimer spectrum, centered near the IETS step voltage, lies outside the IETS framework and makes a quantitative fit to the step position difficult. We note that $S_A = ½$ is identical to the spin of a free Mn atom.

From the excitation spectra of the dimer and trimer, we determined both free parameters J and S_A of the Heisenberg Hamiltonian in Eq. 1. Using these two values, we then calculated the excitation spectra for chains up to $N = 6$ (*35*). For odd-length chains, we found that the ground and first excited states have total spin ½ and ⅔, respectively. In contrast, even-length chains have ground and first excited state spins of 0 and 1, respectively. This result is consistent with the observed parity dependence of the spin-flip feature and with the triplet splitting of the spin-changing excitation of even-length chains. The calculated energy of the first excited state, as shown in Fig. 2, is in very good agreement with the observed spectral features on the longer chains, considering the simplicity of the model.

To further demonstrate the potential to engineer the coupling between atomic spins, we have also built dimers with the same Mn spacing but atop N atoms in the CuN layer. Conductance spectra of such a dimer also show a single IETS step, now at ~3 mV, that splits into three distinct steps in a magnetic field. As seen in fig. S1, the coupling strength in these dimers is half as large as for dimers built atop Cu sites.

We note that only a single spin-flip and a single spin-changing transition were observed on odd-length chains. For example, in the trimer spectra shown in Fig. 3B, only a single IETS step is observed for each type of transition; at large B, the higher energy IETS step does not split into multiple steps but simply shifts to lower energy. Because $S = ½$ for the ground state and ⅔ for the first excited state, we would expect to observe multiple spin-flip and spin-changing transitions in a magnetic field. It is thus likely that some transitions are prohibited by IETS selection rules. By using the spin states determined from the Heisenberg model, we find IETS steps only when $\Delta S = 0, \pm 1$ and $\Delta m = 0, \pm 1$. A more detailed understanding of the inelastic tunneling process may shed light on the origins of these selection rules.

One aspect of the spectra of the Mn chains that is not currently understood is the clear asymmetry with respect to voltage polarity. In the trimer spectrum in Fig. 2, the conductance steps occur at both positive and negative voltages but the step heights are markedly different. This asymmetry enhances features at positive voltages for small chains and then shifts to enhance the negative voltage features on longer chains.

Many of the zero-field 0.6 K results presented here were also observed with our 5.5 K STM, with the expected thermal broadening of the spectra, which implies that useful IETS studies of exchange-coupled magnetic nanostructures may be performed without the requirement of subkelvin instruments. A comparison with ab initio calculations may help to determine the nature of the observed exchange coupling, which could be the result of superexchange through molecular orbitals or mediated by the conduction electrons of the underlying metal substrate.

We have shown that the combination of in situ imaging, atom manipulation, and spin-excitation spectroscopy can be used to assemble and probe magnetic nanostructures. Such structures may serve as new model systems for the exploration of low-dimensional magnetism (*36*), and may be used to realize spin-based computation schemes (*37*) and bistable systems for information storage at the atomic scale.

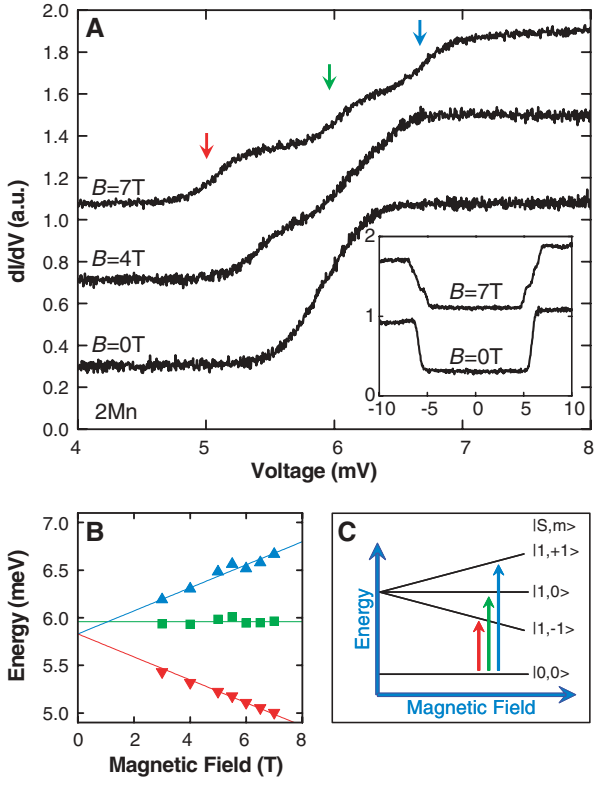

Fig. 4. Conductance spectra of Mn dimer on CuN. (**A**) Spectra taken on a Mn dimer on CuN at $T = 0.6$ K at $B = 0$, 4, and 7 T. All spectra were acquired at a nominal junction impedance of 20 megohms (8 mV, 0.4 nA), and successive spectra are vertically offset by 0.4 units for clarity. Arrows indicate the positions of the low (red), central (green), and high (blue) energy steps from fits of the 7 T spectrum with IETS line shapes (*31*). Inset shows the same spectra, taken at a nominal junction impedance of 50 megohms (20 mV, 0.4 nA), over a larger voltage range. (**B**) Step energies from IETS fits for low (red triangles), central (green squares), and high (blue triangles) energy steps in the dimer spectra as a function of magnetic field. Best fits were obtained with temperatures of ~1.0 K. The uncertainty of the points is typically smaller than the size of the symbols. The solid lines are fits of the step energies to $E_{|\Delta m|} + \Delta m g \mu_B B$, with $g = 2.1 \pm 0.1$, $E_0 = 5.96 \pm 0.05$ meV for $\Delta m = 0$ (green line), and $E_1 = 5.83 \pm 0.05$ meV for $\Delta m = \pm 1$ (blue and red lines). (**C**) Schematic of the energy-level spacing of singlet and triplet states in a magnetic field, labeled by total spin S and magnetic quantum number m. Transitions from the $|0,0\rangle$ singlet state to the $|1,-1\rangle$, $|1,0\rangle$, and $|1,+1\rangle$ triplet states are labeled by red, green, and blue arrows, respectively.

References and Notes

1. S. A. Wolf *et al.*, *Science* **294**, 1488 (2001).
2. M. N. Leuenberger, D. Loss, *Nature* **410**, 789 (2001).
3. F. H. L. Koppens *et al.*, *Science* **309**, 1346 (2005).
4. J. R. Petta *et al.*, *Science* **309**, 2180 (2005).
5. X. Xu, S. Yin, R. Moro, W. A. de Heer, *Phys. Rev. Lett.* **95**, 237209 (2005).
6. P. Gambardella *et al.*, *Nature* **416**, 301 (2002).
7. O. Kahn, *Molecular Magnetism* (Wiley-VCH, New York, 1993).
8. J. R. Friedman, M. P. Sarachik, J. Tejada, R. Ziolo, *Phys. Rev. Lett.* **76**, 3830 (1996).
9. L. Thomas *et al.*, *Nature* **383**, 145 (1996).
10. A. Abragan, B. Bleaney, *Electron Paramagnetic Resonance of Transition Ions* (Clarendon, Oxford, 1970).
11. S. Hill, R. S. Edwards, N. Aliaga-Alcalde, G. Christou, *Science* **302**, 1015 (2003).
12. R. Caciuffo *et al.*, *Phys. Rev. Lett.* **81**, 4744 (1998).
13. D. Rugar, R. Budakian, H. J. Mamin, B. W. Chui, *Nature* **430**, 329 (2004).
14. A. Zhao *et al.*, *Science* **309**, 1542 (2005).
15. V. Madhavan, W. Chen, T. Jamneala, M. F. Crommie, N. S. Wingreen, *Science* **280**, 567 (1998).
16. J. Li, W.-D. Schneider, R. Berndt, B. Delley, *Phys. Rev. Lett.* **80**, 2893 (1998).
17. M. Bode, O. Pietzsch, A. Kubetzka, R. Wiesendanger, *Phys. Rev. Lett.* **92**, 067201 (2004).
18. A. Yamasaki *et al.*, *Phys. Rev. Lett.* **91**, 127201 (2003).
19. A. J. Heinrich, J. A. Gupta, C. P. Lutz, D. M. Eigler, *Science* **306**, 466 (2004).
20. D. M. Eigler, E. K. Schweizer, *Nature* **344**, 524 (1990).
21. T. Jamneala, V. Madhavan, M. F. Crommie, *Phys. Rev. Lett.* **87**, 256804 (2001).
22. H. J. Lee, W. Ho, M. Persson, *Phys. Rev. Lett.* **92**, 186802 (2004).
23. F. M. Leibsle, C. F. J. Flipse, A. W. Robinson, *Phys. Rev. B* **47**, 15865 (1993).
24. Small islands of copper nitride were formed on Cu(100) by nitrogen implantation using a 1-keV beam of N_2 ions followed by annealing to 400°C for 1 min. The sample was then transferred into the precooled STM, and Mn atoms were subsequently evaporated onto the surface.
25. X. H. Qiu, G. V. Nazin, W. Ho, *Science* **299**, 542 (2003).
26. E. Ćavar *et al.*, *Phys. Rev. Lett.* **95**, 196102 (2005).
27. J. Repp, G. Meyer, S. M. Stojković, A. Gourdon, C. Joachim, *Phys. Rev. Lett.* **94**, 026803 (2005).
28. D. M. Eigler, C. P. Lutz, W. E. Rudge, *Nature* **352**, 600 (1991).
29. L. Bartels, G. Meyer, K.-H. Rieder, *Phys. Rev. Lett.* **79**, 697 (1997).
30. Mn was transferred to the tip from either the CuN or bare Cu surface by moving the tip into point contact with the atom and then withdrawing the tip while applying +2 V. The atom was then transferred to the CuN by repeating this procedure with –0.5 V. Mn atoms can bind to the CuN atop either a Cu or N atom, with the Cu site being more stable.
31. J. Lambe, R. C. Jaklevic, *Phys. Rev.* **165**, 821 (1968).
32. B. C. Stipe, M. A. Rezaei, W. Ho, *Science* **280**, 1732 (1998).
33. P. Gambardella *et al.*, *Science* **300**, 1130 (2003).
34. The conductance steps at low fields on Mn atoms and trimers are too narrow to resolve the flat bottom that clearly differentiates an IETS line shape from the Fano line shape that characterizes the Kondo effect (*15*, *16*). Because this flat bottom is seen on longer chains, we consider the Kondo interpretation to be unlikely for the shorter chains as well.
35. Because H_N is represented as a $(2S_A + 1)^N \times (2S_A + 1)^N$ matrix, numerical diagonalization becomes computationally expensive for larger S_A and N. We therefore limited our calculations to $N \leq 6$.
36. L. J. de Jongh, A. R. Miedema, *Adv. Phys.* **23**, 1 (1974).
37. A. Imre *et al.*, *Science* **311**, 205 (2006).
38. N. Nilius, T. M. Wallis, W. Ho, *Science* **297**, 1853 (2002).
39. STM topographic images were processed using WSxM (www.nanotec.es). We thank D. M. Eigler for mentoring and stimulating discussions; B. J. Melior for expert technical assistance; and C.-Y. Lin and B. A. Jones for stimulating discussions.

Supporting Online Material

www.sciencemag.org/cgi/content/full/1125398/DC1
Fig. S1
References and Notes

25 January 2006; accepted 13 March 2006
Published online 30 March 2006;
10.1126/science.1125398
Include this information when citing this paper.

Desorption of H from Si(111) by Resonant Excitation of the Si-H Vibrational Stretch Mode

Zhiheng Liu,[1,2] L. C. Feldman,[2,3] N. H. Tolk,[2] Zhenyu Zhang,[3,4] P. I. Cohen[1]*

Past efforts to achieve selective bond scission by vibrational excitation have been thwarted by energy thermalization. Here we report resonant photodesorption of hydrogen from a Si(111) surface using tunable infrared radiation. The wavelength dependence of the desorption yield peaks at 0.26 electron volt: the energy of the Si-H vibrational stretch mode. The desorption yield is quadratic in the infrared intensity. A strong H/D isotope effect rules out thermal desorption mechanisms, and electronic effects are not applicable in this low-energy regime. A molecular mechanism accounting for the desorption event remains elusive.

Photon-stimulated desorption is a powerful tool to study fundamental processes in adsorbate-surface systems, as well as to achieve selective surface reactions for controlled surface processing (*1*–*4*). Photons are easily directed and tuned in energy to induce transitions in atomic and molecular states, with high spatial and temporal precision. Direct adsorbate-surface bond breaking by electronic excitation using ultraviolet light has been reported (*5*, *6*). However, visible and infrared (IR)–stimulated desorption processes studied so far generally involve indirect mechanisms (*7*, *8*), such as light-induced substrate heating (*9*) and, in physisorbed systems, energy transfer from internal molecular excitation to molecular translational motion away from the surface (*10*, *11*). Selective bond scission at these lower energies is desirable but has proven challenging because of rapid energy delocalization from the mode of excitation (*1*). Here we report resonant photodesorption of H from a Si(111) surface using IR radiation. We show that the process is resonant with the Si-H vibrational energy and displays an unusual and surprising dependence on excitation intensity, which cannot be explained by either thermal or electronic processes. Successful elucidation of this fundamental excitation mechanism would be a major advance in surface science, and its implementation could lead to site-selective desorption at low temperatures.

The H/Si(111) structure is a well-characterized adsorbate system, ideal for the study of fundamental surface processes. The Si-H bond is perpendicular to the Si(111) surface, with a bond energy estimated to be between 3.15 and 3.35 eV (*12*) and a vibrational stretch energy of 0.26 eV at the terrace sites (*13*). In our experiments, the Si-H vibrational stretch mode was resonantly excited by IR photons. The Si substrate was transparent to mid-IR illumination, minimizing electronic excitation and direct laser-induced heating. Although this paper deals with the basic mechanisms of the desorption process, there could be important technological applications. Because H desorption is an important component of Si chemical vapor deposition, modifying the H desorption mechanism can have a large impact on growth. In particular, the vibrational energy of an Si-H bond at the terrace site of the Si(111) surface differs from that at the step site by 51.8 cm^{-1} (*14*), opening the possibility of site-selective desorption of H adatoms by IR irradiation. Such a photolytic process could efficiently treat a large area and modify the type of sites available for epitaxial growth. This might be compared to nanoscale lithography of H on Si achieved using the scanning tunneling microscope (STM) (*15*, *16*).

Our experiment was performed in an ultrahigh-vacuum (UHV) system at room temperature. The base pressure was $\sim 3.0 \times 10^{-10}$ Torr. The sample was prepared in air, using hydrofluoric acid etching to protect the Si surface from oxidation and contamination, and then cleaned by direct-current heating in the UHV chamber. The clean surface was verified by the strong Si(111)-7×7 low-energy electron diffraction (LEED) pattern. Ultrahigh-purity H_2 gas was introduced into the UHV chamber. A tungsten filament at 2000 K was used to dissociate H_2 molecules, thus efficiently forming

[1]Department of Electrical and Computer Engineering, University of Minnesota, Minneapolis, MN 55455, USA. [2]Department of Physics and Astronomy, Vanderbilt University, Nashville, TN 37235, USA. [3]Materials Science and Technology Division, Oak Ridge National Laboratory, Oak Ridge, TN 37831, USA. [4]Department of Physics and Astronomy, University of Tennessee, Knoxville, TN 37996, USA.

*To whom correspondence should be addressed. E-mail: picohen@umn.edu